Geotechnical Testing Journal, Vol. 30, No. 3
Paper ID GTJ100663
Available online at: www.astm.org

Ahmet H. Aydilek,[1] *Douglas D'Hondt,*[2] *and Robert D. Holtz*[3]

Comparative Evaluation of Geotextile Pore Sizes Using Bubble Point Test and Image Analysis

ABSTRACT: Analysis of the filtration performance of a geotextile filter necessitates accurate information about the size distribution of geotextile pore openings. The effectiveness of the bubble point test in determining the pore and constriction sizes of geotextiles was evaluated. The characteristic woven geotextile pore and nonwoven geotextile constriction sizes, O_{95}, were determined for a variety of specimens and compared with both the manufacturers' reported *AOS* values, and with those determined from the two previously developed image-based procedures and theoretical equations. The results indicated that the O_{95} sizes of woven mono and multifilament geotextiles determined by image analyses compared well with the *AOS* values, whereas the same observations were not made for the bubble point-based O_{95} sizes. The O_{95} constriction sizes of various nonwoven geotextiles obtained by the bubble point test were not comparable to the manufacturers' reported *AOS* values, indicating the limitation of ASTM D 4751 in determining constriction sizes. A direct method, such as image analysis, may be a better approach for determining the pore sizes of woven geotextiles, whereas the bubble point method should be preferred to determine constriction sizes in a nonwoven geotextile. Recommendations are made in regard to improvements in the current ASTM standard on bubble point testing.

KEYWORDS: nonwoven geotextile, woven geotextile, pore size, constriction size, image analysis, dry sieving, bubble point

Introduction

Geotextiles are increasingly being used to replace graded granular filters in many drainage applications because of their economy, consistent properties, ease of placement, and comparable performance. However, as with graded granular filters, geotextile filters require a proper engineering design if they are to perform as desired. All of the available methods for designing geotextile filters use grain size parameters determined on the soil to be protected by the filter, and required geotextile characteristics usually include the apparent opening size, *AOS* (ASTM D 4751 2005), and the permittivity (ASTM D 4491 2005) of the geotextile. Some design methods also require a filtration or clogging test, for example, the gradient ratio test (ASTM D 5101 2005) or the hydraulic conductivity ratio test (ASTM D 5567 2005).

Because the flow of water through a soil and a geotextile is really a pore phenomenon, geotextile filter design should fundamentally be based on the pore size distribution of the filter. This would require accurate information about the distribution of pore openings or pore channels in the geotextile filters to be able to properly assess their filtration performance (Bhatia et al. 1993; Bhatia et al. 1996). Another complicating factor is the constriction pore size, especially in nonwoven geotextiles. As defined by Fischer (1994), the constriction pore size is the minimum pore size of a flow channel, and it is the critical parameter in the filtration response of a geotextile. Due to their tortuous flow paths, the constriction pore sizes of nonwoven geotextiles may be located at any depth inside the geotextile. Vermeersch and Mlynarek (1996) and Giroud et al. (1998) have confirmed that constriction sizes of a geotextile impact filtration performance, and if they can be accurately measured, they should be used for the design of geotextile filters. Fischer et al. (1990) and Fischer (1994) have developed a design criterion using the constriction size distribution of nonwoven geotextiles.

Sometimes the dry sieving or *AOS* test (ASTM D 4751) is used to determine pore sizes smaller than the *AOS* or O_{95}. However, this method is not very accurate due to problems in testing procedure (Van der Sluys and Dierickx 1991; Giroud 1996). A better method to determine the pore sizes is the bubble point test. As noted by Fischer (1994), this test determines the constriction pore sizes, albeit indirectly by approximating them from the measured minimum constriction area. ASTM Committee D-35 on Geosynthetics a few years ago adapted with a few changes and limited validation testing the bubble point procedure for membranes, Test Method F 316, to geotextiles as Test Method D 6767 (ASTM D 6767 2005; Fischer 1994; Bhatia and Smith 1996; Bhatia et al. 1996; Vermeersch and Mlynarek 1996). The accuracy of the procedure described in D 6767 has only been verified for pore or constriction sizes up to 200 μm (0.2 mm). The geotextiles used in filtration applications, particularly the wovens, have pore sizes greater than 0.2 mm and applicability of D 6767 to those geotextiles should be evaluated.

An alternative method for determining geotextile pore and constriction sizes is image analysis. Most image analysis methods use two-dimensional planar or cross-sectional view images of a geotextile (Masounave et al. 1980; Rollin et al. 1982; Bhatia et al. 1996; Elsharief and Lovell 1996), and are quite operator-dependent. Moreover, the measurements are image-specific rather than representing the entire geotextile layer. To overcome these shortcomings, Aydilek and Edil (2004) and Aydilek et al. (2005) developed image-based methodologies to determine the pore and constriction sizes of geotextiles. They compared the image-based measurements with the very few bubble point data available.

In response to this lack of comparative data, a research study was undertaken in which both image analysis and bubble point tests were conducted on 29 different woven and nonwoven geotextiles. The characteristic woven geotextile pore and nonwoven geotextile

Manuscript received May 25, 2006; accepted for publication August 10, 2006; published online October 2006.

[1]Assistant Professor, Department of Civil and Environmental Engineering, University of Maryland, 1163 Glenn Martin Hall, College Park, MD 20742, e-mail: aydilek@eng.umd.edu

[2]Department of the Army, Installation Management, Yakima, WA.

[3]Professor, Department of Civil and Environmental Engineering, University of Washington, 132F More Hall, Box 352700, Seattle, WA 98195.

TABLE 1a—*Properties of nonwoven geotextiles tested in the current study.*

Geotextile	Structure, Polymer Type	Mass/Unit Area (g/m^2)	Thickness (mm)	Apparent Opening Size, *AOS* (mm)	Porosity (%)	Permittivity (s^{-1})
NW1	NW, NP, STF, PP	110	1.0	0.3	87.8	2.10
NW2	NW, NP, STF, PP	163	1.40	0.15	87.1	1.80
NW3	NW, NP, STF, PP	217	1.90	0.212	87.3	1.4
NW4	NW, NP, STF, PP	278	2.30	0.15	86.6	1.20
NW5	NW, NP, STF, PP	387	3.0	0.106	85.7	0.80
NW6	NW, NP, STF, PP	492	3.80	0.106	85.6	0.70
NW7	NW, NP, CF, PP	136	1.13	0.212	86.6	2.30
NW8	NW, NP, CF, PP	340	2.53	0.15	85.0	1.10
NW9	NW, NP, CF, PP	401	2.92	0.15	84.7	1.0
NW10	NW, NP, CF, PP	533	3.68	0.106	83.9	0.64
NW11	NW, HB, CF, PP	136	0.45	0.212	66.4	0.7

Notes: NW: nonwoven, W: woven, SF: slit film, MF: monofilament, MU: multifilament, NP: needle-punched, STF: staple fiber, CF: continuous filament, PP: polypropylene. NA: not analyzed, NR: not reported. All properties are the manufacturers' reported values based on the ASTM (2005) standards with the exception of the porosity values, which were determined using the method described by Wayne and Koerner (1993). *AOS* and POA values for Geotextile W1 are based on communication with the manufacturer.

TABLE 1b—*Properties of woven geotextiles tested in the current study.*

Geotextile	Structure, Polymer Type	Mass/Unit Area (g/m^2)	Thickness (mm)	Apparent Opening Size, *AOS* (mm)	Porosity (%)	Permittivity (s^{-1})
W1	W, MF, PP	120	0.53	0.65	53	NA
W2	W, MF, PP	192	0.35	0.425	10	0.95
W3	W, MF, PP	204	0.66	0.425	20	2.14
W4	W, MF, PP	207	0.61	0.425	10	1.36
W5	W, MF, PP	218	0.56	0.425	NR	0.5
W6	W, MF, PP	240	0.27	0.212	4	0.28
W7	W, MF, PP	340	0.39	0.3	NR	0.04
W8	W, MF, PP	490	NA	0.6	NR	0.40
W9	W, MU, PP	257	0.65	0.6	8	1.50
W10	W, MU, PP	285	0.45	0.425	6	0.96
W11	W, MF/MU, PET	850	2.0	0.15	NR	0.07
W12	*W*, SF, PP	102	0.16	0.425	1	0.15
W13	W, SF, PP	151	0.33	0.3	2	0.07
W14	W, SF, PP	165	0.32	0.3	1	0.05
W15	W, SF, PP	224	0.41	0.212	4	0.28
W16	W, SF, PP	225	0.57	0.3	5	0.5
W17	W, SF, PP	263	0.46	0.425	1	0.05
W18	W, SF, PP	291	0.60	0.425	1	0.09

Notes: NW: nonwoven, W: woven, SF: slit film, MF: monofilament, MU: multifilament, NP: needle-punched, STF: staple fiber, CF: continuous filament, PP: polypropylene. NA: not analyzed, NR: not reported. All properties are the manufacturers' reported values based on the ASTM (2005) standards with the exception of the porosity values, which were determined using the method described by Wayne and Koerner (1993). *AOS* and POA values for Geotextile W1 are based on communication with the manufacturer.

constriction sizes, O_{95}, were compared with each other as well as with manufacturers' reported *AOS* values and the predictions of two theoretical equations, and the results are presented in this paper. The image-based procedures used were developed by Aydilek and Edil (2004) and Aydilek et al. (2005), and the bubble point tests essentially followed ASTM D 6767 (D'Hondt 2005).

Materials and methodology

Geotextiles

Eighteen woven and eleven nonwoven geotextiles were selected for comparison testing. Many are commonly used as filters, but they also had a wide range of percent open area (POA), apparent opening size (*AOS* or O_{95}), and permittivity values. The wovens included monofilaments, multifilaments, and slit-films. One of the nonwovens was a heat-bonded geotextile, while all the others were needle-punched, and included both staple fiber and continuous filament geotextiles. The physical and hydraulic properties of the geotextiles are given in Table 1a and 1b.

Bubble Point Test

Figure 1 shows both a schematic diagram and a photograph of the test equipment used to perform the bubble point tests. The procedures outlined in ASTM D 6767 for the bubble point testing of the geotextiles were generally followed. The wetting liquid used was deionized water because validation tests performed by D'Hondt

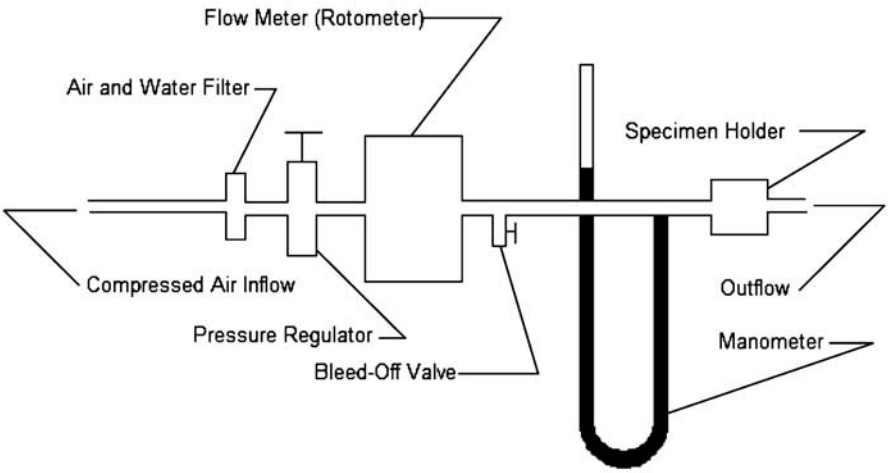

(a)

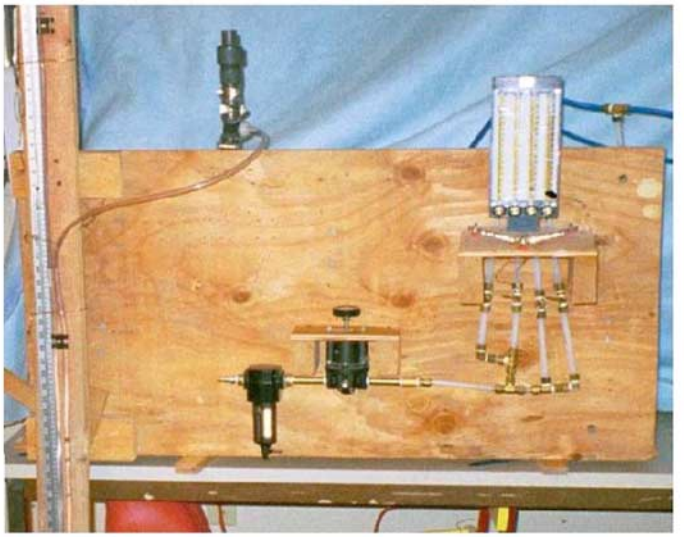

(b)

FIG. 1—(*a*) *A schematic, and* (*b*) *a photograph of the bubble point test equipment.*

(2005) using deionized water, glycerin, and mineral oil on geotextile NW5 indicated that the constriction sizes determined with water were more repeatable than with the other liquids. Another complicating factor is that the contact angles between geosynthetic polymers and mineral oil and glycerin are unknown.

D'Hondt (2005) also made other refinements to the bubble point test equipment and procedure followed by Fischer (1994) to improve the accuracy and repeatability of the tests. A bleed valve was installed between the specimen holder and the flow meters. This valve relieved any air pressure that developed during specimen installation. Furthermore, the flow meters did not have sufficient capacity to measure the airflow in the system through the 25-mm diameter geotextiles specimens. To solve this problem, nylon flat washers with a 12-mm center hole were placed on each side of the geotextile specimen to reduce the airflow, and O-rings were installed between the washers and the specimen holder to prevent air loss around the perimeters of the washers. The washers created a large orifice and fluid flow, such as the airflow in the bubble point test, through the orifice created turbulence. However, preliminary tests conducted on plastic and metal disks with holes of known size and orientation indicated that the large orifice did not appear to affect the accuracy of the geotextile pore sizes (D'Hondt 2005).

ASTM D 6767 does not explicitly require that a contact angle be used for the specific polymer or liquid; however, the procedure states that the contact angle will influence the results. Henry and Patton (1998) showed that omitting the contact angle can overestimate the pore size by a factor of two. For contact with water, they measured the contact angle for polypropylene to be 86° advancing and 54° receding, and for polyester, it was 76° advancing and 63° receding. The advancing contact angle occurs when fluid and the specimen contact each other, whereas a receding contact angle is developed as the fluid is removed from the specimen when the bubble point test is performed. Since the bubble point test determines pore size by mobilizing sufficient air pressure to force the test liquid out of the geotextile pores, receding contact angle values were used in the pore size calculations.

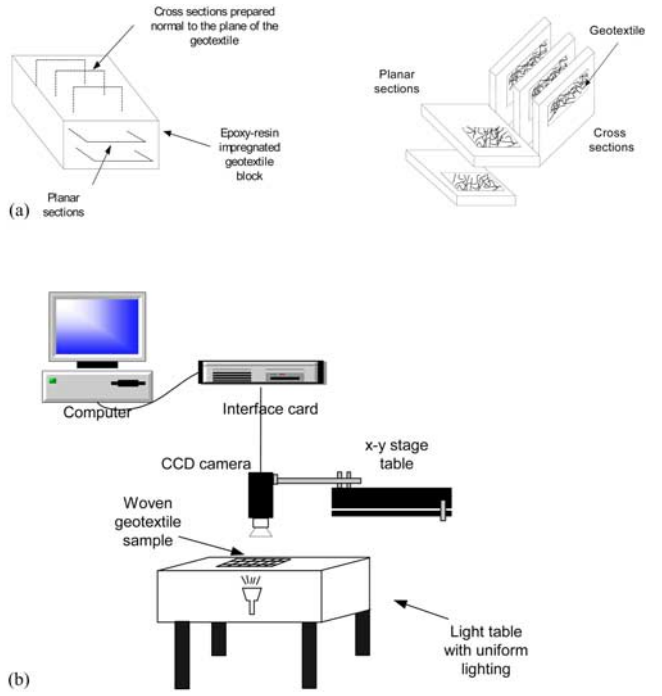

FIG. 2—(*a*) *Specimen preparation for nonwoven geotextiles, and* (*b*) *image analysis setup for woven geotextiles.*

Image Analysis

The three-dimensional structure of nonwoven geotextiles presents difficulties in observing pore structures under a light microscope. Planar and cross-sectional thin sections are necessary to provide detailed three-dimensional information. The thin sectioning process involved planar sections as well as sections normal to the plane of the geotextile. The latter were termed cross sections. From each geotextile type, three sets of specimens were prepared, with each specimen yielding three cross-sectional and two planar sections (underlying planar sections) (Fig. 2(*a*)). The thin sections of the geotextiles investigated in this research were prepared following the procedures generally used for preparing thin sections of soil and rock. This required a series of steps: epoxy-resin impregnation, cutting, grinding, lapping, and polishing. Aydilek et al. (2002) provides details of the specimen preparation technique.

Images of woven geotextiles were captured by using an image analysis system that included a charged couple device (CCD) analog camera, high precision x-y stage table, and a light table providing a light intensity of 2000 lumens. Figure 2(*b*) provides a schematic diagram of the setup. The images of nonwoven geotextiles were captured using an optical light microscope having a macro zoom lens, digital camera coupled with image-capturing software.

A code named PORE and written in MATLAB was used for PSD determination of woven geotextiles. The flow chart of the algorithm is shown in Fig. 3. A detailed explanation and validation of PORE are given in Aydilek and Edil (2004). Unlike the evaluation of the woven geotextiles, the captured images of nonwoven geotextiles required further processing, e.g., image filtering and slicing. The information obtained from the processed two-dimensional images were then input into a probabilistic model that determined the constriction sizes of the channels, i.e., the smallest pore diameter in the channel, and plotted their distributions (constriction size distributions, CSDs). A flow chart of the methodology is given in Fig. 4.

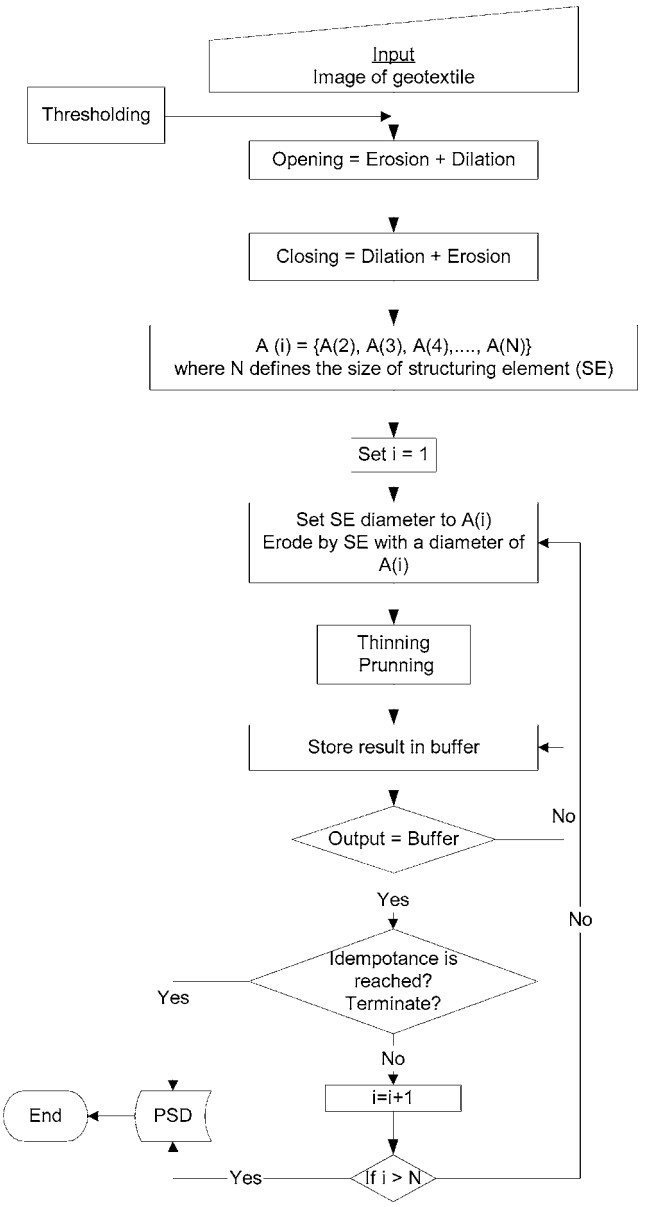

FIG. 3—*Image analysis methodology for the woven geotextiles.*

Aydilek et al. (2002) and Aydilek et al. (2005) provide a detailed explanation of the methods used to process the images and determine CSDs.

Results and Discussion

Comparison of Measured Pore and Constriction Sizes with the Reported Sizes

Table 2a and 2b summarizes the manufacturers' reported *AOS* values and the O_{95} values measured in the bubble point tests and image analyses. The bubble point-based O_{95}s for five out of the eleven nonwoven geotextiles (NW2, NW7, NW8, NW9, and NW10) are somewhat comparable with the manufacturers' reported *AOS* values. Similarly, only four of the 18 woven geotextiles (W7, W11, W15, and W16) exhibited comparable bubble point-based O_{95} and

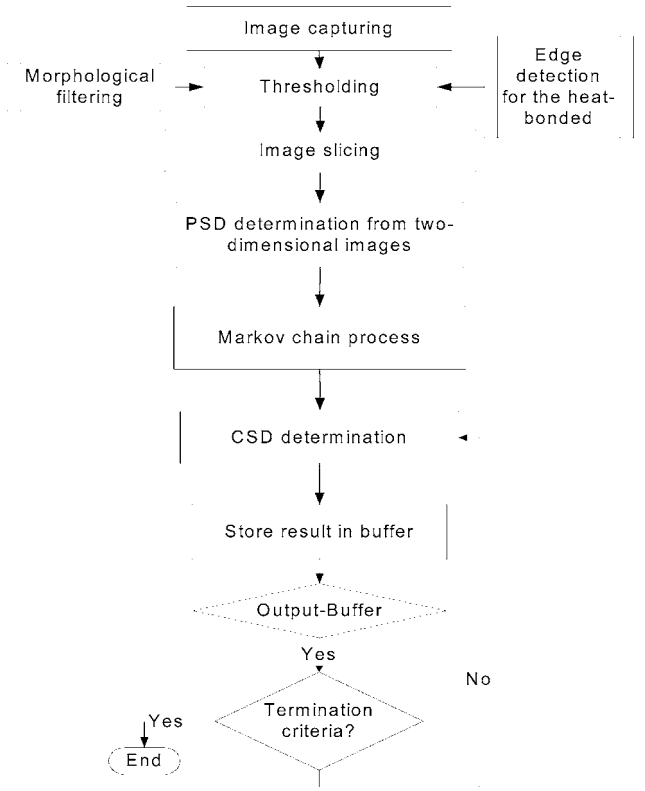

FIG. 4—*Image analysis methodology for the nonwoven geotextiles.*

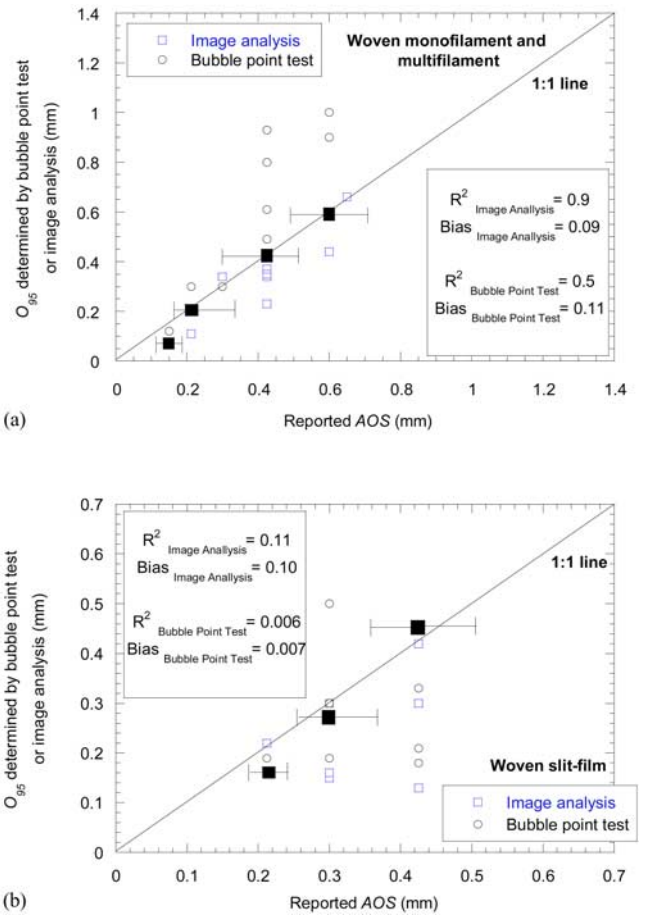

FIG. 5—*Bubble point-based and image-based O_{95} values versus AOS for (a) slit film, and (b) monofilament and multifilament wovens. Solid squares represent the manufacturers' AOS, and the error bars indicate the range of bead sizes defined in ASTM D 4751.*

AOS values. The relatively large pore openings in geotextile W1 (POA=53 %) created problems during the bubble point test as a sufficient quantity of flow could not be sustained. Thus, this geotextile was eliminated from the testing program.

The apparent opening size (*AOS*) of a geotextile is included in most of the existing filter design criteria because it represents the largest hole in the geotextile, and this value—analogous to D_{85} in graded granular filters—controls retention (prevention of piping) rather well. Further, there is a standard test procedure available for determination of *AOS* by dry sieving glass beads, i.e., ASTM D 4751. However, the test method has been criticized by Mlynarek et al. (1993) and Bhatia and Smith (1996) because of electrostatic effects, sagging of the geotextile in the support frame, and unspecified vibration frequency. Moreover, the range between the bead sizes specified in ASTM D 4751 is too large. For instance, if a particular bead size tested gives the O_{80}, the next specified bead size might easily give O_{98}, which, however, will be reported as O_{95}. For this research, a conservative approach was taken and, in addition to manufacturers' reported *AOS* values, the range of bead sizes given in ASTM D 4751 were compared with the bubble point-based or image-based sizes. Figures 5 and 6 show these comparisons for wovens and nonwovens, respectively.

The O_{95} sizes of monofilament and multifilament geotextiles determined by image analysis compare reasonably well with the manufacturers' reported *AOS* values. The R^2 values are lower for the slit films due to their more heterogeneous structures (R^2=0.9 and monofilaments and multifilaments, and 0.11 for slit films, respectively). However, it is important to note that the R^2 slightly increases to 0.95 for mono and multiflaments and significantly increases to 0.64 for slit films (Aydilek and Edil 2004) when the lower end of the range of bead sizes defined in D 4751 is used rather than the manufacturers' reported sizes (i.e., the lower end of the error bars in Fig. 5). These observations clearly demonstrate the shortcomings of the D 4751 in accurately defining the O_{95} sizes. Figure 5(*b*) also shows that the bubble point-based O_{95} sizes of woven slit films are not comparable with the *AOS* (R^2=0.006). This is somewhat consistent with the observations made by Fischer (1994) that the test method may produce poor results for woven geotextiles, since relatively high airflow through these geotextiles may overpredict the pore sizes. This overprediction in the bubble point test is also pronounced for the monofilament and multifilament geotextiles tested in the current study due to their large pore sizes (Table 2a and 2b and Fig. 5). These findings suggest that a direct method such as image analysis may be a more accurate approach for determining the pore sizes of woven geotextiles, particularly the monofilament and multifilament ones, due to their two-dimensional structure and the presence of relatively large pore openings.

The data in Table 2a and 2b and Fig. 6 indicate that the image-based O_{95} sizes of nonwoven geotextiles do not compare well with the reported *AOS* values. The R^2 values are 0.39 and 0.49 for staple fiber and continuous filament geotextiles, respectively. The bubble point-based O_{95} sizes compare somewhat better with the reported *AOS*s; however, the observed R^2 values are still low (0.44 and 0.65, respectively). Even though the variability in geotextile samples used in two different tests (bubble point and dry sieving) due to manufacturing and random locations of the fibers may have caused

TABLE 2a—*O_{95} of nonwoven geotextiles tested in the current study.*

Geotextile	Structure	Thickness (mm)	Fiber Diameter (μm)	Apparent Opening Size, *AOS* (mm)	Bubble Point-based O_{95} (mm)	Image-based O_{95} (mm)
NW1	NW, NP, STF	1.0	30.5	0.3	0.15–0.23	NA
NW2	NW, NP, STF	1.40	31.8	0.15	0.16	0.09
NW3	NW, NP, STF	1.90	33.8	0.212	0.13–0.18	NA
NW4	NW, NP, STF	2.30	30.1	0.15	0.12–0.13	0.073
NW5	NW, NP, STF	3.00	31.2	0.106	0.073–0.088	0.05
NW6	NW, NP, STF	3.80	31.1	0.106	0.12–0.18	0.078
NW7	NW, NP, CF	1.13	30.3	0.212	0.20–0.22	0.09
NW8	NW, NP, CF	2.53	35.4	0.15	0.13–0.18	0.082
NW9	NW, NP, CF	2.92	30.2	0.15	0.15–0.16	0.08
NW10	NW, NP, CF	3.68	33.1	0.106	0.08–0.11	0.07
NW11	NW, HB, CF	0.45	43.4	0.212	0.39–0.43	0.12

Notes: NW: nonwoven, W: woven, SF: slit film, MF: monofilament, MU: multifilament, NP: needle-punched, STF: staple fiber, CF: continuous filament, PP: polypropylene. NA: not analyzed, NR: not reported, NM: image-based measurements of pore size was not possible due to the structure of geotextile, NT: test could not be conducted since the flow exceeded the capacity of the flowmeter. All properties are the manufacturers' reported values based on the ASTM (2005) standards with the exception of the porosity values, which were determined using the method described by Wayne and Koerner (1993), and the fiber diameters were measured using image analysis. *AOS* and POA values for Geotextile W1 are based on communication with the manufacturer.

TABLE 2b—*O_{95} of woven geotextiles tested in the current study.*

Geotextile	Structure	Thickness (mm)	Fiber Diameter (μm)	Apparent Opening Size, *AOS* (mm)	Bubble Point-based O_{95} (mm)	Image-based O_{95} (mm)
W1	W, MF	0.533	0.65	NT	0.66	
W2	W, MF	0.354	0.425	0.80	0.37	
W3	W, MF	0.664	0.425	0.45–0.49	0.34	
W4	W, MF	0.613	0.425	0.61	0.23	
W5	W, MF	0.564	0.425	0.91–0.93	0.23	
W6	W, MF	0.272	0.212	0.28–0.31	0.11	
W7	W, MF	0.394	0.3	0.3–0.31	0.34	
W8	W, MF	NR	0.6	0.99–1.0	NM	
W9	W, MU	0.645	0.6	0.90–0.94	0.44	
W10	W,MU	0.454	0.425	NA	0.35	
W11	W, MF/MU	2.0	0.15	0.12–0.45	NM	
W12	*W*, SF	0.163	0.425	0.33–0.34	0.3	
W13	W, SF	0.330	0.3	0.50–0.67	0.15	
W14	W, SF	0.316	0.3	0.19–0.28	0.16	
W15	W, SF	0.406	0.212	0.19	0.22	
W16	W, SF	0.572	0.3	0.3	0.3	
W17	W, SF	0.462	0.425	0.18–0.20	0.13	
W18	W, SF	0.603	0.425	0.21–0.22	0.42	

Notes: NW: nonwoven, W: woven, SF: slit film, MF: monofilament, MU: multifilament, NP: needle-punched, STF: staple fiber, CF: continuous filament, PP: polypropylene. NA: not analyzed, NR: not reported, NM: image-based measurements of pore size was not possible due to the structure of geotextile, NT: test could not be conducted since the flow exceeded the capacity of the flowmeter. All properties are the manufacturers' reported values based on the ASTM (2005) standards with the exception of the porosity values, which were determined using the method described by Wayne and Koerner (1993), and the fiber diameters were measured using image analysis. *AOS* and POA values for Geotextile W1 are based on communication with the manufacturer.

the observed differences in test results, the data clearly reveal that the constriction sizes measured by bubble point tests are different than the *AOS*.

Comparison of Bubble Point-Based Sizes with Image-Based and Theoretical Sizes

It is well known that the thickness of a nonwoven geotextile has a direct effect on its filtration properties, and it is often considered in design, for example, in determining the permittivity. In order to observe this effect, thicknesses are plotted versus the measured constriction sizes in Fig. 7, which also shows the predicted values of O_{95} based on two theoretical equations developed by previous researchers. The first equation proposed by Giroud (1996) is based on the porosity, thickness, and fiber diameter of a nonwoven geotextile:

$$\frac{O_f}{d_f} = \frac{1}{\sqrt{1-n}} - 1 + \frac{\xi n d_f}{(1-n)t} \tag{1}$$

where d_f is the fiber thickness, n is porosity, t is geotextile thickness, and O_f is the filtration opening size and is usually given by the nearly largest constriction size of a particular geotextile (e.g., O_{95}).

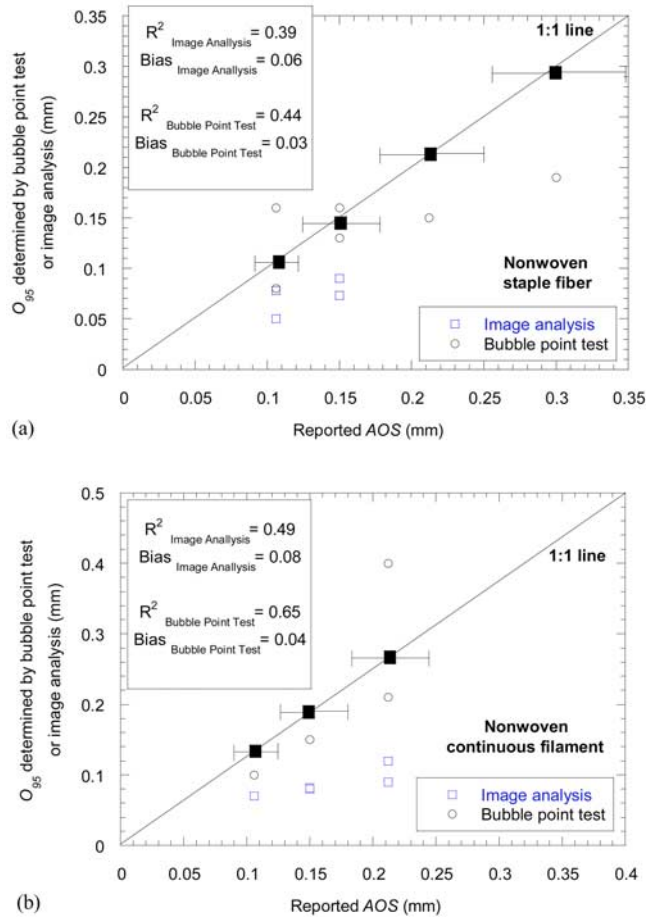

FIG. 6—*Bubble point-based and image-based O_{95} values versus AOS for* (*a*) *staple fiber, and* (*b*) *continuous filament nonwovens. Solid squares represent the manufacturers' AOS, and the error bars indicate the range of bead sizes defined in ASTM D 4751.*

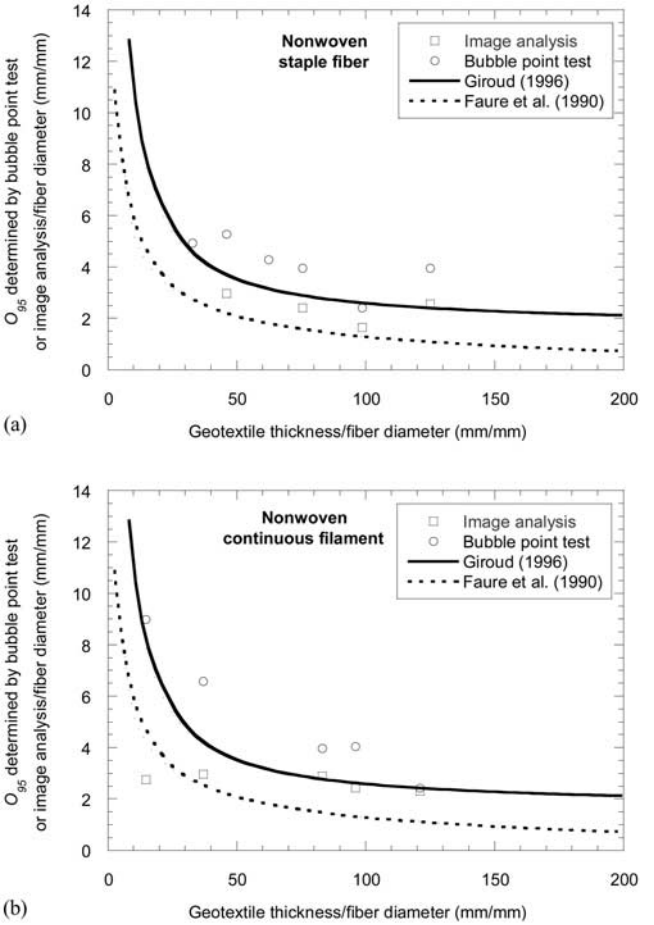

FIG. 7—*Bubble point-based and image-based O_{95} values versus thickness for* (*a*) *staple fiber, and* (*b*) *continuous filament nonwovens.*

The parameter ξ is dimensionless and was taken as 10 as suggested by Giroud (1996). The second equation was developed by Faure et al. (1990) based on a Poissonian polyhedra model and is given below:

$$P_f(d) = n\left[\frac{2\lambda(d + + d_f)}{2 + \lambda d_f}\right]^{2N} \exp^{(-N\lambda d)} \quad (2)$$

where $P_g(d)$ is the probability of a particle with a diameter d passing through a pore channel in the geotextile, n is the porosity of the geotextile, λ is total length of straight lines per unit area in a planar surface (also termed as specific length), and N is number of slices in a cross-sectional image. A detailed explanation of the two techniques is provided by Giroud (1996).

An analysis of data in Fig. 7 indicates that the O_{95} pore sizes tend to decrease with increasing thickness, and the trend is more clearly pronounced in the bubble point test data. Furthermore, the O_{95} sizes determined from the two methods follow a decreasing trend somewhat similar to the one defined by Giroud's theoretical curve. The relatively good predictions of the bubble point test data made by the theoretical equation are also consistent with the findings of Aydilek et al. (2005). As expected, the Faure et al. (1990) approach generally produces lower values than ones measured by these three approaches due to an assumption that at relatively high geotextile thicknesses the constriction size tends to approach zero. The results presented in Fig. 7 also show that the image-based O_{95} pore sizes are consistently lower than their bubble point-based companions.

Figure 8 shows the difference in the constriction size distributions of four different geotextiles determined with image analyses and bubble point tests. The image-based distributions are shifted to the left as compared to the CSD of the geotextile determined from the bubble point test. The observations made in Fig. 8 are consistent with the findings of Aydilek et al. (2005) that the smaller pore sizes (e.g., O_{20}, O_{50}) measured by image analysis are generally lower than those ones measured in the bubble point test. It is believed that many factors including disturbance during specimen preparation for the image analysis, approximations associated with thresholding and other image processing algorithms, and assumptions made during the development of the probabilistic model may have contributed to the observed differences (Aydilek et al. 2005).

Summary and Conclusions

A study was conducted to evaluate the effectiveness of the bubble point test in determining the pore and constriction sizes of geotextiles. Bubble point tests were performed on 29 different geotextiles. The characteristic woven geotextile pore and nonwoven geotextile constriction sizes, O_{95}, were determined for a variety of specimens and compared with manufacturers' reported *AOS* values. The same

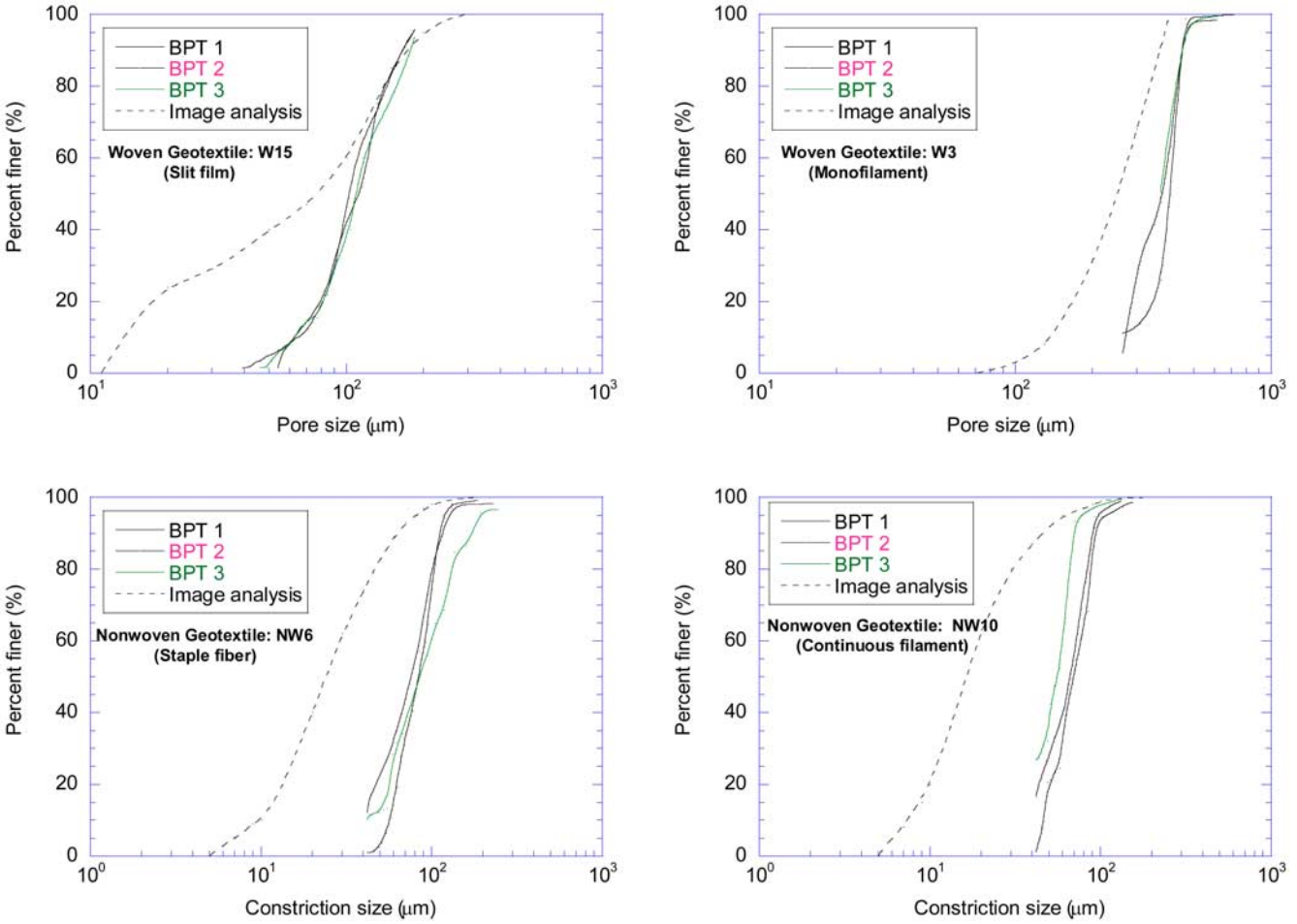

FIG. 8—*Comparison of CSDs of four geotextiles determined via bubble point test and image analysis.*

sizes were also compared with those determined from two previously developed image-based procedures and theoretical equations.

The results indicated that the O_{95} sizes of woven mono and multifilament geotextiles determined by image analysis compared reasonably well with the manufacturers' reported *AOS* values, whereas this was not the case for the bubble point-based O_{95} sizes. A direct method such as image analysis may be a better approach for determining the pore sizes of woven geotextiles due to their two-dimensional structure and the presence of relatively large pore openings. The O_{95} constriction sizes of various nonwoven geotextiles obtained by the bubble point test were not comparable to the manufacturers' reported *AOS* values, indicating the limitation of the ASTM D 4751 *AOS* test procedure in determining constriction sizes. Further, the image-based O_{95} constriction sizes were somewhat lower than those from the bubble point test, most probably due to disturbance in specimen preparation and assumptions inherent to the image-based probabilistic model.

The two theoretical equations, Faure et al. (1990) and Giroud (1996), produced constriction sizes somewhat lower than the ones measured in the bubble point tests; however, similar trends were observed when the constriction sizes were plotted versus geotextile thicknesses.

The current study suggests that the ASTM D 6767 bubble point test is the best available test to determine constriction sizes in a nonwoven geotextile. However, it is recommended that ASTM D 6767 should be revised to include variable contact angles for different test fluids and polymers. Additionally, the method currently does not consider temperature variations during testing, which may have an effect on capillarity and therefore constriction sizes. Moreover, the test equipment should be modified to accommodate compressed specimens since it is widely known that the pressure required to force the test liquid from the sample changes with varying specimen thickness.

Acknowledgments

The authors would like to thank Dr. Gregory R. Fischer for his helpful discussions during the project. Various manufacturers provided the geotextiles at no cost and their support is appreciated.

References

ASTM Standard D 4491, 2005, "Standard Test Methods for Water Permeability of Geotextiles by Permittivity," *Annual Book of ASTM Standards*, ASTM International, West Conshohocken, PA.

ASTM Standard D 5101, 2005, "Standard Test Method for Measuring the Soil-Geotextile System Clogging Potential by the Gradi-

ent Ratio," *Annual Book of ASTM Standards*, ASTM International, West Conshohocken, PA.

ASTM Standard D 4757, 2005, "Standard Test Method for Determining Apparent Opening Size of a Geotextile." *Annual Book of ASTM Standards*, ASTM International, West Conshohocken, PA.

ASTM Standard D 5567, 2005, "Standard Test Method for Hydraulic Conductivity Ratio (HCR) Testing of Soil/Geotextile Systems," *Annual Book of ASTM Standards*, ASTM International, West Conshohocken, PA.

ASTM Standard D 6767, 2005, "Standard Test Method for Pore Size Characteristics of Geotextiles by Capillary Flow Test," *Annual Book of ASTM Standards*, ASTM International, West Conshohocken, PA.

Aydilek, A. H. and Edil, T. B., 2004, "Pore Structure Parameters of Woven Geotextiles," *Geotech. Test. J.*, Vol. 27, No. 1, pp. 99–110.

Aydilek, A. H., Oguz, S. H., and Edil, T. B., 2002, "Digital Image Analysis to Determine Pore Opening Size Distribution of Nonwoven Geotextiles," *J. Comput. Civ. Eng.*, ASCE, Vol. 16, No. 4, pp. 280–290.

Aydilek, A. H., Oguz, S. H., and Edil, T. B., 2005, "Constriction Size of Geotextile Filters," *J. Geotech. Geoenviron. Eng.*, ASCE, Vol. 131, No. 1, pp. 28–38.

Bhatia, S. K. and Smith, J. L., 1996, "Geotextile Characterization and Pore Size Distribution: Part II. A Review of Test Methods and Results," *Geosynthet. Int.*, IFAI, Vol. 3, No. 2, pp. 155–180.

Bhatia, S. K., Huang, Q., and Smith, J. L., 1993, "Application of Digital Image Processing in Morphological Analysis of Geotextiles," *Proceedings of the Conference on Digital Image Processing: Techniques and Applications in Civil Engineering, Special Publication*, ASCE, Honolulu, HI, Vol. 1, pp. 71–80.

Bhatia, S. K., Smith, J. L., and Christopher, B. R., 1996, "Geotextile Characterization and Pore Size Distribution: Part III. Comparison of Methods and Application to Design," *Geosynthet. Int.*, IFAI, Vol. 3, No. 3, pp. 301–328.

D'Hondt, D. P., 2005, "An Investigation of the Pore Size Distribution of Geotextiles and Other Materials by the Bubble Point Method," MSE Thesis, University of Washington, Seattle, WA, 153 pp.

Elsharief, A. M. and Lovell, C., 1996, "Determination and Comparisons of the Pore Structure of Nonwoven Geotextiles," *Recent Developments in Geotextile Filters and Prefabricated Drainage Geocomposites*, ASTM STP 1281, S. K. Bhatia and L. D. Suits, Eds., ASTM International, West Conshohocken, PA, pp. 35–55.

Faure, Y. H., Gourc, J. P., and Gendrin, P., 1990, "Structural Study of Porometry and Filtration Opening Size of Geotextiles," *Geosynthetics: Microstructure and Performance*, ASTM STP 1076, I. D. Peggs, Ed., ASTM International, West Conshohocken, PA, pp. 102–119.

Fischer, G. R., 1994, "The Influence of Fabric Pore Structure on the Behavior of Geotextile Filters," Ph.D. Dissertation, University of Washington, Seattle, WA, 501 pp.

Fischer, G. R., Holtz, R. D., and Christopher, B. R., 1990, "Filter Criteria Based on Pore Size Distribution," *Proceedings of the 4th International Conference on Geotextiles, Geomembranes and Related Products*, The Hague, Netherlands, Vol. 1, pp. 289–294.

Giroud, J. P., 1996, "Granular Filters and Geotextile Filters," *Proceedings of Geofilters '96*, Montreal, Canada, pp. 565–680.

Giroud, J. P., Delmas, P., and Artières, O., 1998, "Theoretical Basis for the Development of a Two-Layer Geotextile Filter," *Proceedings of the 6th International Conference on Geosynthetics*, Atlanta, GA, pp. 1037–1044.

Henry, K. S. and Patton, S., 1998, "Measurement of the Contact Angle of Water on Geotextile Fibers," *Geotech. Test. J.*, Vol. 21, No. 1, pp. 11–17.

Masounave, J., Denis, R., and Rollin, A. L., 1980, "Prediction of Hydraulic Properties of Synthetic Nonwoven Fabrics Used in Geotechnical Work," *Can. Geotech. J.*, Vol. 17, pp. 517–525.

Mlynarek, J., Lafleur, J., Rollin, A., and Lombard, G., 1993, "Filtration Opening Size of Geotextiles by Hydrodynamic Sieving," *Geotech. Test. J.*, Vol. 16, No. 1, pp. 61–69.

Rollin, A. L., Denis, R., Estaque, L., and Masounave, J., 1982, "Hydraulic Behavior of Synthetic Non-Woven Filter Fabrics," *Can. J. Chem. Eng.*, Vol. 60, pp. 226–234.

Van der Sluys, L. and Dierickx, W., 1990, "Comparative Studies of Different Porometry Determination Methods for Geotextiles," *Geotext. Geomembr.*, Vol. 9, pp. 183–198.

Vermeersch, O. G. and Mlynarek, J., 1996, "Determination of the Pore Size Distribution of Nonwoven Geotextiles by a Modified Flow Porometry Technique," *Recent Developments in Geotextile Filters and Prefabricated Drainage Geocomposites, ASTM STP 1281*, S. K. Bhatia and L. D. Suits, Eds., ASTM International, West Conshohocken, PA, pp. 19–34.

Wayne, M. H., and Koerner, R. M., 1994, "Correlation between Long-Term Flow Testing and Current Geotextile Filtration Design Practice," *Proceedings of Geosynthetics '93*, Vancouver, Canada, pp. 501–517.